

# Chapter 4

## Thrust Network Analysis for Masonry Assessment



Ricardo Maia Avelino, Tom Van Mele, and Philippe Block

**Abstract** This chapter presents Thrust Network Analysis (TNA), a lower-bound limit-analysis-based method to assess vaulted masonry structures. With TNA, admissible equilibrium states corresponding to compressive force networks within the structural geometry can be studied. A novel multi-objective optimisation framework is described, which enables finding particular admissible equilibrium solutions in 3D structures subjected to general loading and support displacements. The equilibrium solutions searched include the minimum and maximum horizontal thrust states, the minimum vault thickness, maximum vertical and horizontal collapse loads, and compatible internal stress states following support movements. A complete picture of the structure's stability level is obtained by combining these states, and the location where cracks arise at limit states is also highlighted. The method can be applied based on the surveyed geometric data of the structure's envelope, being well-suitable for practical engineering problems. Analysis of shallow cross vaults and a surveyed cathedral demonstrate the method's applicability and its relevance to assessing vaulted masonry structures.

### 4.1 Introduction

Masonry structures form a large part of the world's built heritage and serve as housing for millions worldwide. Moved by the pressing need for a more sustainable built environment and heritage protection, research on the analysis and preservation of existing masonry buildings has grown recently (Angelillo et al., 2021; Funari et al.,

---

R. Maia Avelino · T. Van Mele · P. Block (✉)

Block Research Group, Institute of Technology in Architecture, Department of Architecture, ETH Zurich, Zurich, Switzerland  
e-mail: [block@arch.ethz.ch](mailto:block@arch.ethz.ch)

R. Maia Avelino  
e-mail: [maia@arch.ethz.ch](mailto:maia@arch.ethz.ch)

T. Van Mele  
e-mail: [van.mele@arch.ethz.ch](mailto:van.mele@arch.ethz.ch)

2021; Mehrotra et al., 2023). Novel analysis tools and methods have been conceived to determine their level of stability and resistance against the actions of exceptional actions such as seismic and wind loads (D'Altri et al., 2019; Tralli et al., 2014).

From a mechanics point of view, the highly nonlinear, discrete and unilateral behaviour of masonry structures precludes the use of general analysis tools without proper consideration of either material properties or specific modelling of the internal joints (Aita et al., 2015; Huerta, 2008; Shin et al., 2016). Consequently, different approaches have been adopted for the structural analysis of masonry, such as the Discrete Element Method (DEM) (Cundall, 1971; Lemos, 2007, 2019), nonlinear Finite Element Method (FEM) (Lourenço and Rots, 1997; Milani et al., 2008; Parisi et al., 2019; Smoljanović et al., 2013) and Limit Analysis (LA) based approaches (Heyman, 1966, 1995). This contribution focuses on the latter, which offers a framework for computing collapse loads or collapse mechanisms in structures supported by geometry-based information, i.e., without relying on mechanical properties, such as compressive strength and stiffness, which are often unknown or unknowable.

Limit Analysis is a branch of plastic analysis which searches for limit states in the structure instead of computing the elastic deformations throughout the material. It was initially applied to the design of steel frames (Baker et al., 1956; Prager, 1959) and extended to masonry by Heyman (1966) by assuming infinite compressive strength, null tensile capacity and no-sliding failure. Two approaches can be adopted to apply LA: lower-bound approaches, based on the Safe Theorem (Block and Ochsendorf, 2002; Fraddosio et al., 2019; Heyman, 1969), and upper-bound approaches (Chiozzi et al., 2017; Grillanda et al., 2019).

By applying the Safe Theorem to masonry, admissible stress states are characterised as compressive force paths within the structural geometry and in equilibrium with externally applied loads. For two-dimensional structures, these compressive force path result in the so-called thrust lines, applied to arches (Moseley, 1843), sliced domes (Poleni, 1748) and vaults (Ungewitter, 1890), and commonly applied in combination with graphic statics (e.g., Wolfe, 1921). Currently, this technique is known as Thrust Line Analysis (TLA), and it has been extended to a few three-dimensional problems, such as the dome under symmetric loading cases (Aita et al., 2019; Zessin et al., 2010), vaults (Smars, 2000) and spiral staircases (Angelillo et al., 2021). TLA is also the core of 2D masonry analysis tools such as LimitState (LimitState Ltd, 2020) and Archie-M (Obvis, 2016).

Nevertheless, extending lower-bound methods to fully three-dimensional structures is challenging due to the increased degree of indeterminacy and the complex geometry of masonry vaults (Huerta, 2008). Therefore, various lower-bound equilibrium formulations have recently been developed to assess three-dimensional masonry structures. These strategies can be divided into continuous and discrete approaches.

Continuous approaches model the internal forces of the structure as a continuous membrane with the equilibrium equations solved by assuming a Pucher formulation and considering the potential stress (or Airy) functions to describe the internal distribution of the stresses (Angelillo et al., 2013; Fraddosio et al., 2020; Fraternali, 2010).

Discrete approaches consider a singular internal stress field discretised by a network (O'Dwyer, 1999; Block and Ochsendorf, 2007). The compressive forces are modelled as axial forces along the network's edges, and loads are applied to its vertices. The equilibrium equations are linearised with discrete approaches, and geometric irregularities, concentrated loads, and openings can be directly investigated.

A discrete network approach was proposed initially in O'Dwyer (1999). In Block and Ochsendorf (2007), this approach was combined with graphic statics (Culmann, 1875), with the introduction of Thrust Network Analysis (TNA). With TNA, the spatial equilibrium of the networks is explored by the reciprocal relations of form and force diagrams analogous to the force polygons in graphic statics (Block, 2009). The problem can also be formulated based on the Force Density Method (Schek, 1974) in which the force densities at the edges of the network are variables of the equilibrium equations. Using this formulation, TNA has been coupled with optimisation procedures and applied to masonry assessment problems (Block and Lachauer, 2014; Bruggi, 2020; Maia Avelino et al., 2021a, 2022a). In Block and Lachauer (2014), networks with fixed horizontal projections are considered for which the degrees of freedom of the network can be explicitly defined with the independent edges (Van Mele and Block, 2014). This formulation has been applied to find the minimum and maximum thrust states (Bruggi, 2020), compute the structure's Geometric Safety Factor (GSF) (Maia Avelino et al., 2021a), and find specific internal stress states arising after differential foundation displacements (Maia Avelino et al., 2022a). Other researchers have also considered problems with disconnected networks (Fantin and Ciblac, 2016; Nodargi and Bisegna, 2022), which enlarge the solution space but require additional friction checks on the interface of the nodes.

This book chapter revisits the TNA formulation used to find admissible equilibrium states in masonry structures. It presents a modular multi-objective optimisation formulation (Maia Avelino, 2023), which enables finding multiple admissible equilibrium states with a unique approach. This modular framework can be applied to determine the structural safety levels and the structural response to external actions such as support displacements and vertical and horizontal live loads.

This paper is organised as follows: Sect. 4.2 presents TNA and the numerical formulation applied to explore the geometry of thrust networks, Sect. 4.3 presents the constrained optimisation framework to find particular equilibrium solutions, Sect. 4.4 shows applications of the method to vaulted masonry structures, and Sect. 4.5 concludes this paper by summarising the results presented and pointing to further research.

## 4.2 Thrust Network Analysis

This section describes a numerical formulation to find thrust networks. The main elements of TNA are defined in Sect. 4.2.1. The equilibrium equations for finding the geometry of the network based on its internal force densities are described in Sect. 4.2.2. The particular case of networks fixed in the plan is discussed in Sect. 4.2.3,

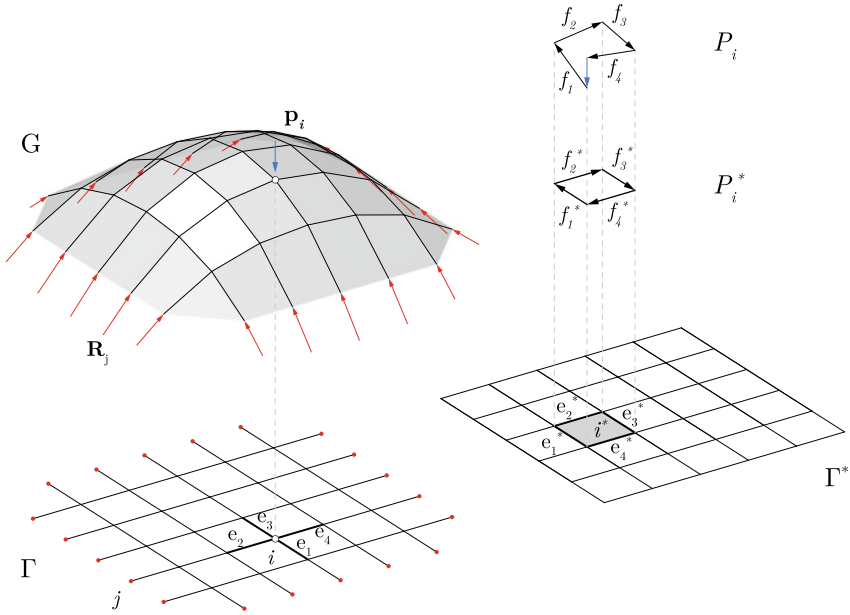


**Fig. 4.1** Thrust Network (G) with its horizontal projection, the form diagram ( $\Gamma$ ). Equilibrium  $P_i$  of node  $i$  subjected to the vertical applied load  $\mathbf{p}_i$  is highlighted. The horizontal projection of  $P_i$  is the closed polygon  $P_i^*$ . Summing the polygons, the network’s force diagram ( $\Gamma^*$ ) is obtained

and strategies to handle the degrees of freedom in these cases are presented in Sect. 4.2.4.

### 4.2.1 Main Elements

This section defines the main elements of Thrust Network Analysis (TNA), after (Block, 2009), which are illustrated in Fig. 4.1.

A thrust network (G) is a *directed* and *connected* spatial graph in which the edges of G represent the spatial compressive resultants (or thrusts) within the structure.

The form diagram ( $\Gamma$ ) is a planar graph constructed from the projection of G. The form diagram stores the network’s topology, connectivity, and planar coordinates. Each vertex  $i$  in the form diagram with coordinates  $(x_i, y_i)$  maps to a vertex in the thrust network with elevation  $z_i$ . Similarly, each edge  $e_i$  in the form diagram maps to an edge in the thrust network carrying axial force  $f_i$ .

Boundary conditions and loads are applied to the nodes of the network. For example, Fig. 4.1 highlights the support points in the form diagram with a red dot, where reaction forces  $\mathbf{R}_j$  arise. An external vertical load  $\mathbf{p}_i$  applied to node  $i$  is also high-

lighted. The equilibrium of the node can be verified through the construction of closed polygons of force vectors  $P_i$  indicated in Fig. 4.1.

The force diagram ( $\Gamma^*$ ) is a graphical representation of the horizontal equilibrium of  $G$ . When all loads are parallel, the spatial equilibrium of a node  $i$  can be projected onto a plane perpendicular to the loads resulting in a two-dimensional graphic statics problem. In Fig. 4.1, the projected equilibrium of node  $i$  is the closed polygon  $P_i^*$  where the vertical applied load  $\mathbf{p}_i$  vanishes. The horizontal equilibrium is then resolved with the horizontal components of the thrusts ( $f_i^*$ ). The form ( $\Gamma$ ) and force ( $\Gamma^*$ ) diagrams are reciprocal, such that their corresponding edges  $e_i$ ,  $e_i^*$  are parallel, and the length of  $e_i^*$  is proportional to the horizontal force  $f_i^*$ .

The geometry of thrust networks can be explored by searching and modifying the reciprocal form and force diagrams, as proposed in Block et al. (2019), Rippmann et al. (2012) using a parallelisation algorithm. Recently, new computational tools have been developed to provide interactive access to this process, such as RhinoVault (Block Research Group, 2021; Rippmann, 2016). This pipeline has been adopted to the conceptual design stage of several shell prototypes and projects, e.g., the Striatum Bridge (Bhooshan et al., 2022) and Armadillo Vault (Block et al., 2018).

Nevertheless, fitting this network within a (usually tight) structural envelope is required for masonry assessment, which requires robust optimisation strategies and suitable problem parametrisation. Furthermore, the graphic-statics-based TNA framework is limited to vertical loading cases, so horizontal forces can not be applied. The following section presents a numerical description of the network's equilibrium based on force densities which enables general loading cases and is suitable for numerical optimisation.

## 4.2.2 Equilibrium Equations

This section presents the equilibrium formulation in general force networks based on force densities (Schek, 1974).

A network composed of  $m$  edges and  $n$  vertices is considered, with  $n_b$  supported vertices and  $n_i$  free vertices, such that  $n = n_i + n_b$ . The nodal positions of the network are cast in the vectors  $\mathbf{x}$ ,  $\mathbf{y}$ ,  $\mathbf{z}$  [ $n \times 1$ ], and the applied forces in each direction are collected in  $\mathbf{p}_x$ ,  $\mathbf{p}_y$ ,  $\mathbf{p}_z$  [ $n \times 1$ ]. The equilibrium variables are the force densities  $\mathbf{q}$  [ $m \times 1$ ] defined for each edge as the ratio between its axial force  $f_i$  and its length  $l_i$ .

The equilibrium equations can be written by introducing the connectivity matrix  $\mathbf{C}$  [ $m \times n$ ] (see Schek, 1974) and defining the coordinate difference matrices  $\mathbf{U} = \text{diag}(\mathbf{C}\mathbf{x})$ ,  $\mathbf{V} = \text{diag}(\mathbf{C}\mathbf{y})$ ,  $\mathbf{W} = \text{diag}(\mathbf{C}\mathbf{z})$ . The  $3n_i$  linear internal equilibrium equations become

$$\mathbf{C}_i^T \mathbf{U} \mathbf{q} = \mathbf{p}_{x,i}, \quad (4.1a)$$

$$\mathbf{C}_i^T \mathbf{V} \mathbf{q} = \mathbf{p}_{y,i}, \quad (4.1b)$$

$$\mathbf{C}_i^T \mathbf{W} \mathbf{q} = \mathbf{p}_{z,i}, \quad (4.1c)$$

where,  $\mathbf{C}_i [m \times n_i]$  and  $\mathbf{p}_{x,i}, \mathbf{p}_{y,i}, \mathbf{p}_{z,i}, [n_i \times 1]$  are slices of the connectivity matrix and applied loads in the  $n_i$  free nodes.

At the supported boundaries, the emerging reaction forces  $\mathbf{R}_i = [R_{x,i}; R_{y,i}; R_{z,i}]$  can be retrieved from the reaction components  $\mathbf{R}_x, \mathbf{R}_y, \mathbf{R}_z [n_b \times 1]$  calculated as

$$\mathbf{R}_x = \mathbf{C}_b^T \mathbf{U} \mathbf{q} - \mathbf{p}_{x,b}, \quad (4.2a)$$

$$\mathbf{R}_y = \mathbf{C}_b^T \mathbf{V} \mathbf{q} - \mathbf{p}_{y,b}, \quad (4.2b)$$

$$\mathbf{R}_z = \mathbf{C}_b^T \mathbf{W} \mathbf{q} - \mathbf{p}_{z,b}. \quad (4.2c)$$

where  $\mathbf{C}_b [m \times n_b]$ , and  $\mathbf{p}_{x,b}, \mathbf{p}_{y,b}, \mathbf{p}_{z,b} [n_b \times 1]$  are slices of the connectivity matrix and applied loads in the  $n_b$  supported nodes.

With this formulation, the infinite space of equilibrium networks for a given topology (or connectivity) can be explored in terms of the position of the supports  $\mathbf{x}_b, \mathbf{y}_b, \mathbf{z}_b$  and values of the force densities in the edges of the network  $\mathbf{q}$ , resulting in  $3n_b + m$  parameters.

A subspace of this equilibrium is explored with TNA, considering the cases where the horizontal projection of the network, i.e., the form diagram, is fixed, as introduced in Block and Lachauer (2014). The following section presents the consequence of this assumptions.

### 4.2.3 The Case of a Fixed Form Diagram

By considering the form diagram fixed in the analysis, the planar coordinates of the network  $\mathbf{x}, \mathbf{y}$  are known, and the horizontal equilibrium equations (4.1a) and (4.1b) can be rearranged, introducing the horizontal equilibrium matrix  $\mathbf{E} [2n_i \times m]$  and the vector of applied horizontal forces in the internal nodes  $\mathbf{p}_{h,i} [2n_i \times 1]$ ,

$$\mathbf{E} \mathbf{q} = \mathbf{p}_{h,i}, \quad \text{with: } \mathbf{E} = \begin{bmatrix} \mathbf{C}_i^T \mathbf{U} \\ \mathbf{C}_i^T \mathbf{V} \end{bmatrix}, \quad \mathbf{p}_{h,i} = \begin{bmatrix} \mathbf{p}_{x,i} \\ \mathbf{p}_{y,i} \end{bmatrix}. \quad (4.3)$$

Assuming that the form diagram is fixed imposes additional constraints to the vector of force densities, such that its components can not be chosen freely. Indeed, the number of force densities that can be chosen freely in Eq. 4.3 corresponds to the number  $k$  of degrees of freedom (DOF), or the degree of statical indeterminacy, of the network.

As shown in Van Mele and Block (2014), the number of DOF is equal to the rank deficiency of the matrix  $\mathbf{E}$ . The free parameters are denoted *independent force densities*, and they relate to specific *independent edges* in the network. The independent force densities  $\mathbf{q}_{\text{id}} [k \times 1]$  are then used to describe the force densities  $\mathbf{q}$  in the network through the linear transformation

$$\mathbf{q} = \mathbf{B}\mathbf{q}_{\text{id}} + \mathbf{d}, \text{ with: } \mathbf{B} = \begin{bmatrix} -\mathbf{E}_{\text{d}}^{\dagger}\mathbf{E}_{\text{id}} \\ \mathbf{I}_k \end{bmatrix}, \mathbf{d} = \begin{bmatrix} \mathbf{E}_{\text{d}}^{\dagger}\mathbf{p}_{\text{h,i}} \\ \mathbf{0} \end{bmatrix}, \quad (4.4)$$

where  $\mathbf{E}_{\text{d}} [2n_i \times (m - k)]$  and  $\mathbf{E}_{\text{id}} [2n_i \times k]$  are slices of  $\mathbf{E}$  related to the dependent and independent edges, respectively,  $\mathbf{E}_{\text{d}}^{\dagger}$  is the generalised inverse or Moore-Penrose pseudo-inverse of  $\mathbf{E}_{\text{d}}$ , and  $\mathbf{I}_k$  is the identity matrix of size  $k$ .

After such variable reduction, the elevation of the free nodes in the network  $\mathbf{z}_i$  is a function of  $\mathbf{q}_{\text{id}}$  and  $\mathbf{z}_b$ , resulting in

$$\mathbf{z}_i(\mathbf{q}_{\text{id}}, \mathbf{z}_b) = \mathbf{D}_i^{-1}(\mathbf{p}_{z,i} - \mathbf{D}_b\mathbf{z}_b), \quad (4.5)$$

where  $\mathbf{D}_i = \mathbf{C}_i^T\mathbf{Q}\mathbf{C}_i [n_i \times n_i]$ ,  $\mathbf{D}_b = \mathbf{C}_b^T\mathbf{Q}\mathbf{C}_b [n_b \times n_b]$  and  $\mathbf{Q} = \text{diag}(\mathbf{q}) [m \times m]$ .

With this approach, the number of variables of the problem reduces to  $n_b + k$ . Equation 4.5 will be used to compute the free nodal elevations enabling the constraint optimisation framework described in Sect. 4.3.

#### 4.2.4 Independent Edges in Form Diagrams

As presented in Sect. 4.2.3, the number of independent force densities  $k$  that can be chosen freely in Eq. 4.3 correspond to the dimension of the nullspace of  $\mathbf{E}$  computed as

$$k = m - \text{rank}(\mathbf{E}). \quad (4.6)$$

Therefore, finding a set of independent edges in the network is equivalent to finding one base of the nullspace of  $\mathbf{E}$ . A sequential Singular Value Decomposition (SVD) approach is applied, as described in Maia Avelino et al. (2021a), to find a base of  $k$  linearly independent columns of the nullspace  $\mathbf{E}$  that relate to  $k$  independent edges in the network. As discussed in Liew et al. (2019), these groups are not unique and can not be selected randomly for non-triangulated topologies.

The result of this process is illustrated in four networks in Fig. 4.2, where one of the infinite possible groups of independent edges for each topology is depicted with  $k < m$ .

In Fig. 4.2, (a) the orthogonal form diagram with  $n_d = 6$  divisions has  $m = 60$  edges and  $k = 10$  independent edges, (b) the radial diagram with three hoops and 12 meridians has  $m = 84$  and  $k = 13$ , (c) the cross diagram with  $n_d = 6$  divisions has  $m = 96$  and  $k = 8$ , and (d) the three-sided diagram presents  $m = 42$  and  $k = 4$ .

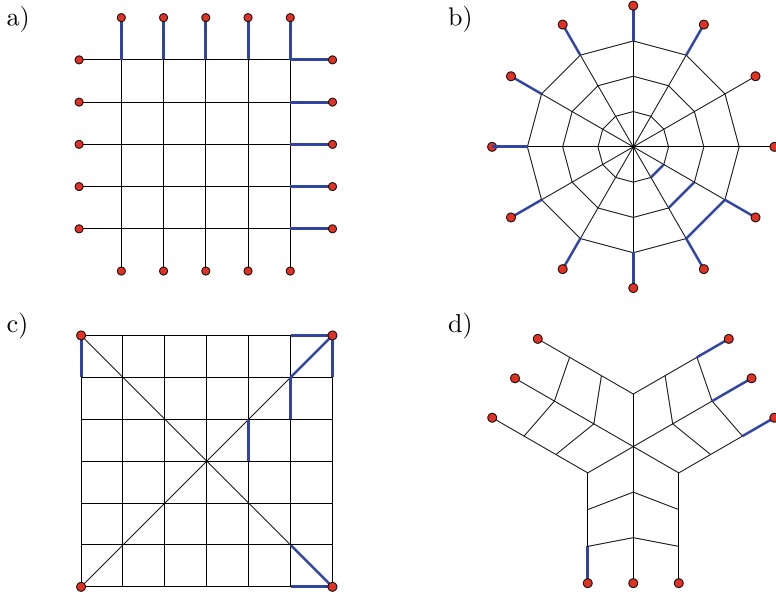


**Fig. 4.2** Independent edges highlighted in blue for different topologies: **a** an orthogonal grid, **b** a radial arrangement, **c** a cross diagram, and **d** a three-sided diagram

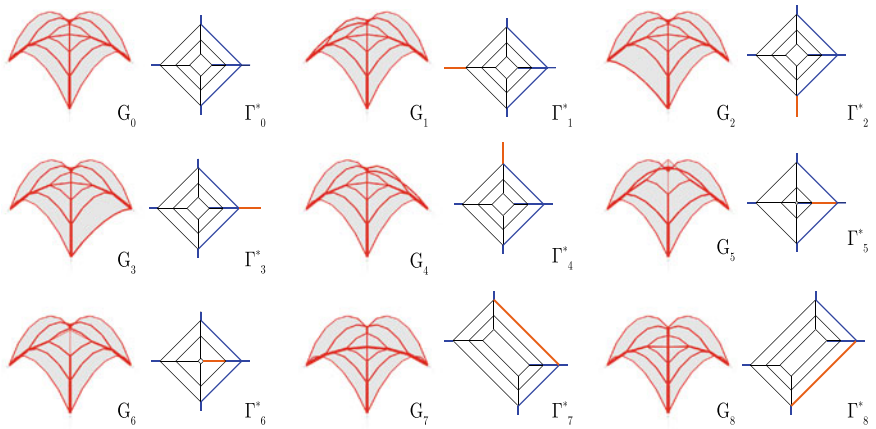


**Fig. 4.3** Individual effect of increasing the force magnitude of the independent edges on the cross form diagram. Modified thrust network ( $G_i$ ) and force diagrams ( $\Gamma_i^*$ ) are shown, highlighting the  $i$ th independent modified

The infinite space of equilibrium networks having a fixed horizontal projection can be explored using this formulation by combining the effect of each independent edge in the final geometry. For example, Fig. 4.3 shows the effect of increasing the force in the  $i$ th independent edge in the thrust network geometry ( $G_i$ ) for the cross form diagram (Fig. 4.2c). The corresponding force diagram ( $\Gamma_i^*$ ) is depicted for each ( $G_i$ ). In  $\Gamma_i^*$ , the force increase is evident by the stretch of the  $i$ th reciprocal independent edge, highlighted in orange (see Fig. 4.3).

The following section introduces the search of admissible thrust networks as a constrained nonlinear optimisation problem assuming the parametrisation in independent edges.

### 4.3 Constrained Equilibrium

This section computes admissible thrust networks through a constrained nonlinear optimisation framework that takes the general form below:

$$\text{minimise}_{\tilde{\mathbf{x}}} \quad f_{\text{obj}}(\tilde{\mathbf{x}}) \quad (4.7a)$$

$$\text{subject to} \quad g_i(\tilde{\mathbf{x}}) \geq 0, \quad \text{for } i = [1, \dots, n_c], \quad (4.7b)$$

where the  $n_c$  inequality constraints translate the limit analysis assumptions for admissible networks, as listed in Sect. 4.3.1. Different objective functions  $f_{\text{obj}}$  are implemented, as defined in Sect. 4.3.2. The optimisation variables  $\tilde{\mathbf{x}}$  correspond to the independent force densities  $\mathbf{q}_{\text{id}}$  and the support elevations  $\mathbf{z}_b$  (see Sect. 4.2.3) followed by occasional auxiliary variables depending on the selected objective (see Sect. 4.3.2).

#### 4.3.1 Constraints from Limit Analysis

As described in Heyman (1966), limit analysis can be applied to masonry structures given that infinite compressive and null tensile strength are assumed, and no sliding failure can occur. In continuum mechanics, these assumptions are generalised in applying the normal, rigid, no-tension material (NRNT) described in Angelillo et al. (2018). For the present formulation, these assumptions translate into no-tensile axial forces at the network edges and in constraining the network to remain within the structural section. The former enforces negative axial force densities  $q_i$  in the edges (Eq. 4.8a). The latter is implemented by constraining the nodal elevations  $z_i$  to lay between the elevations of intrados  $z_i^{\text{LB}}$  and extrados  $z_i^{\text{UB}}$  (Eq. 4.8b).

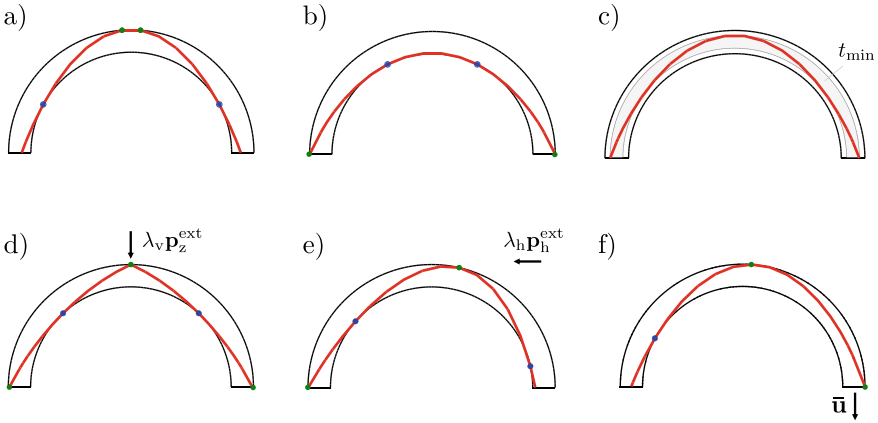


**Fig. 4.4** Examples of different objective functions on a semicircular arch: **a** minimum thrust, **b** maximum thrust, **c** minimum thickness  $t_{\min}$ , **d** maximum vertical load multiplier  $\lambda_v$  associated to an external vertical load  $\mathbf{p}_z^{\text{ext}}$ , **e** maximum horizontal load multiplier  $\lambda_h$  associated to an external horizontal load  $\mathbf{p}_h^{\text{ext}}$  and **f** minimum complementary energy for boundary displacement  $\bar{\mathbf{u}}$

$$q_i \leq 0 \quad \text{for} \quad i = [1, \dots, m], \quad (4.8a)$$

$$z_i^{\text{LB}} \leq z_i \leq z_i^{\text{UB}} \quad \text{for} \quad i = [1, \dots, n]. \quad (4.8b)$$

Additional constraints can be applied, i.e. by limiting the extension of the reaction forces to cross the extrados, as detailed in Maia Avelino et al. (2021a), which is required to model problems such as domes and buttressed vaults.

### 4.3.2 Objective Functions

Different objective functions ( $f_{\text{obj}}$ ) are coupled to the optimisation problem in Eqs.4.7. Figure 4.4 illustrates the different objective functions on a semi-circular arch.

In Fig.4.4, the points in which the thrust line touches the extrados (resp. intrados) are marked in green (resp. blue). They indicate the location where cracks are expected in the solution. When the thrust touches the intrados (resp. extrados), a crack will form in the extrados (resp. intrados).

The objective functions implemented and illustrated in Fig.4.4 are defined mathematically in the following subsections below.

**(a) Minimum horizontal thrust:** Minimises the horizontal component of the emerging reactions  $\mathbf{R}_x$ ,  $\mathbf{R}_y$ , such that the objective function becomes

$$f_{\min} = \sum_{i=1}^{n_b} \sqrt{R_{x,i}^2 + R_{y,i}^2}. \quad (4.9)$$

**(b) Maximum horizontal thrust:** Maximises the horizontal component of the emerging reactions  $\mathbf{R}_x$ ,  $\mathbf{R}_y$ , which is equivalent to minimising the opposite of  $f_{\min}$ , resulting in

$$f_{\max} = - \sum_{i=1}^{n_b} \sqrt{R_{x,i}^2 + R_{y,i}^2}. \quad (4.10)$$

**(c) Minimum structural thickness:** Minimises the additional variable  $t > 0$  representing the structural thickness in the vault computed orthogonally to the masonry's middle surface as

$$f_{\text{thk}} = t. \quad (4.11)$$

Consequently, the additional variable will influence the bounds of the intrados and extrados, modifying the constraint Eq. 4.8b, which will take the form of

$$z_i^{\text{LB}}(t) \leq z_i \leq z_i^{\text{UB}}(t) \quad \text{for} \quad i = [1, \dots, n]. \quad (4.8b)$$

**(d) Maximum vertical load multiplier:** Maximises the vertical load multiplier ( $\lambda_v \geq 0$ ) for a given vertical applied load case  $\mathbf{p}_z^{\text{ext}}$ . The objective function becomes

$$f_v = -\lambda_v. \quad (4.12)$$

The external load and multiplier are then added to the computation of the nodal network elevations in Eq. 4.5, resulting in

$$\mathbf{z}_i(\mathbf{q}_{\text{id}}, \mathbf{z}_b, \lambda_v) = \mathbf{D}_i^{-1} ((\mathbf{p}_{z,i} + \lambda_v \mathbf{p}_{z,i}^{\text{ext}}) - \mathbf{D}_b \mathbf{z}_b). \quad (4.5)$$

**(e) Maximum horizontal load multiplier:** Maximises the horizontal load multiplier ( $\lambda_h \geq 0$ ) for a given horizontal external load case  $\mathbf{p}_h^{\text{ext}}$ , such that the objective function becomes simply

$$f_h = -\lambda_h. \quad (4.13)$$

As a collateral effect, adding this variable modifies the horizontal equilibrium of the structure (Eq. 4.3), now computed as

$$\mathbf{q}(\mathbf{q}_{\text{id}}, \lambda_h) = \mathbf{B} \mathbf{q}_{\text{id}} + \lambda_h \mathbf{E}_d^\dagger \begin{bmatrix} \mathbf{p}_{h,i}^{\text{ext}} \\ \mathbf{0} \end{bmatrix}. \quad (4.3)$$

Furthermore, as discussed in Bruggi (2020), the application of horizontal loads at fixed form diagrams requires that the loads can be transferred appropriately to the supports, which can be verified mathematically by ensuring that the rank of  $\mathbf{E}$  is not modified by stacking the horizontal load case  $\mathbf{p}_{h,i}^{\text{ext}}$ .

**(f) Minimum complementary energy:** Minimises the complementary energy  $W_c$  for a general foundation settlement  $\bar{\mathbf{u}}$  [ $n_b \times 3$ ] which is equal to minimising the opposite work of the reaction forces (Iannuzzo et al., 2020). The objective function becomes

$$f_c = W_c = - \sum_i^{n_b} \mathbf{R}_i \cdot \bar{\mathbf{u}}_i. \quad (4.14)$$

These different objective functions can be added to the optimisation framework in Eq. 4.7. One application for each objective is illustrated in Sect. 4.4.

### 4.3.3 Solving Strategies and Starting Points

The optimisation problem is solved using interior point methods, using the open-source solver IPOPT (Wächter and Biegler, 2006). All analyses presented in this chapter have been conducted with the Python-package *compas\_tno* (Maia Avelino, 2022). *compas\_tno* formulates the constrained optimisation problem (Eq. 4.7), calls the solver, and post-process the final results back into the new geometry of the network.

The starting point of the analysis is the compression-only load-path optimisation described in Liew et al. (2018). This problem corresponds to a convex problem described in Maia Avelino (2023). The result of this pre-conditioning optimisation is a compression-only network that does not yet fit the bounds of the structure. By applying the constraints defined in Sect. 4.3.1, an admissible network is retrieved if the problem is feasible.

The Jacobian matrix and gradients of the constraints and objective functions are defined analytically and passed to IPOPT during the solving process. Jacobian construction and different gradient functions are defined in Maia Avelino (2023).

## 4.4 Applications

This Section shows applications of the modular multi-objective optimisation framework described in vaulted masonry structures. Section 4.4.1 defines the geometry of a shallow cross vault that will be used throughout Sects. 4.4.2–4.4.6, where different assessment problems are tackled by setting different objective functions in the framework. Finally, Sect. 4.4.7 discussed the application of the method from a geometry extracted from point clouds.

### 4.4.1 Vault Geometry

A square shallow cross vault is considered based on the parametric study from Maia Avelino et al. (2021b). The geometry is defined by the vault's base length ( $l_0$ ), (central) radius ( $R$ ), springing angle ( $\beta$ ) and thickness ( $t$ ). The ratio  $r/l_0$  generates pointed ( $r/l_0 > 0.5$ ) or rounded cross vaults ( $r/l_0 = 0.5$ ), and based on the springing angle  $\beta$ , shallower cross vaults can be considered. Whenever  $\beta > 0$ , the effective span ( $s$ ) marks the distance among the springs. The thickness of the structure is referred to by the adimensional  $t/s$ . The parameters of the model are highlighted in Fig. 4.5a. Figure 4.5b shows the cross vault selected for this study with  $r/l_0 = 0.5$ ,  $\beta = 30^\circ$ ,  $t = 0.5$  m and  $s = 10.0$  m.

A density of  $\rho = 20$  kN/m<sup>3</sup> is assumed for the masonry, resulting in a total self-weight of the structure equals  $W = 1088$  kN. The form diagram selected in the following analysis is the cross orthogonal topology presented in Fig. 4.2c with a level of discretisation  $n_d = 16$ , representing 16 divisions of the diagonal.

### 4.4.2 Computing the Extremes of Thrust

This section analyses the vaulted geometry defined in Sect. 4.4.1, finding its minimum and maximum horizontal thrust states. The horizontal thrust is transferred only through the corners of the vault, such that no thrust is transmitted along its open edges.

To obtain the minimum thrust solution, the optimisation in Eq. 4.7 is solved by selecting  $f_{\min}$  as the objective function (Eq. 4.9). The solution is depicted in Fig. 4.6a. In the plots, the thickness of the edges in the thrust network is proportional to the force carried such that edges having zero force are not shown. Furthermore, the points where the network touches the extrados of the vault are highlighted in green, and the points where it touches the intrados are highlighted in blue. At the minimum thrust state, the deepest network is obtained. The network touches the extrados along the

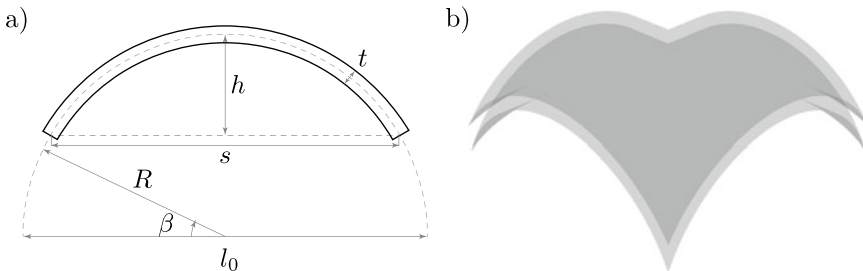


**Fig. 4.5** **a** Parameters used to define the cross vault. **b** Cross vault obtained with  $t/s = 0.05$ ,  $r/l_0 = 0.5$  and  $\beta = 30^\circ$

midspan of the vault, indicating cracks in the intrados of the structure. The value of overall thrust-over-weight obtained is  $T_{\min}/W = 0.97$ , resulting in a horizontal thrust exerted of  $T_{\min} = 1055$  kN for this problem.

Conversely, the maximum thrust state is found by taking as the objective function  $f_{\max}$  (Eq. 4.10). The solution is depicted in Fig. 4.6b. The network assumes its shallowest geometry touching the intrados along the midspan, indicating a crack appearing in the extrados of the cross vault. As a result, the value of the thrust-over-weight is  $T_{\max}/W = 1.57$ , resulting in a horizontal thrust exerted of  $T_{\max} = 1708$  kN.

### 4.4.3 Stability Domain

This section computed the Geometric Safety Factor (GSF) and the stability domain of the shallow cross vault described in Sect. 4.4.1, measuring the level of stability in the structure. After Heyman (1969), the GSF is computed as the ratio between the actual structural thickness ( $t_0$ ) and the minimum thickness of the structure ( $t_{\min}$ ).

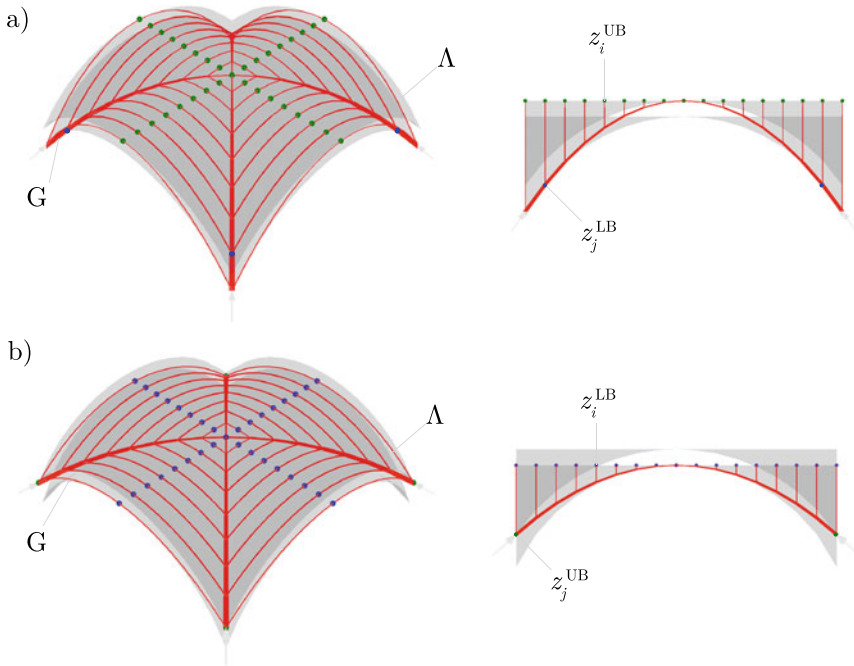


**Fig. 4.6** **a** Minimum thrust solution for the shallow vault with  $T/W = 0.97$ ; **b** Maximum thrust solution for the shallow vault with  $T/W = 1.57$ . Points where the network touches the intrados ( $z_i^{LB}$ ) and extrados ( $z_j^{UB}$ ) are highlighted in blue and green, respectively

To obtain the GSF, the constrained optimisation problem in Eq. 4.7 is solved with the minimum thickness  $f_{thk}$  objective (Eq. 4.11). The minimum thickness value of  $t_{min} = 0.151$  m is obtained, resulting in the network and tightened structural envelope depicted in Fig. 4.7. The GSF is computed, resulting in  $GSF = t_0/t_{min} = 3.3$ . From Heyman (1969), masonry is considered to present a sufficient safety level if the thrust line (or network) is found within the middle third of the structural section (i.e.,  $GSF \geq 3.0$ ). From this benchmark, we can assume that this shallow vault with  $t_0/s = 0.05$  is safe.

Beyond computing the GSF, an additional measure of stability can be obtained by looking at the structure’s stability domain (Maia Avelino et al., 2021a, 2021b). This domain serves as a measure of the infinite space of admissible stress states arising at the structure. It is obtained by computing the minimum and maximum horizontal thrusts (as in Sect. 4.4.2) for decreasing thicknesses of the structure until the minimal thickness  $t_{min}$ . The stability domain for the cross vault analysed is depicted in Fig. 4.8.

Indeed, the area among the maximum and minimum thrust lines stores all possible internal states for the structure that can be evaluated with a given form diagram. As

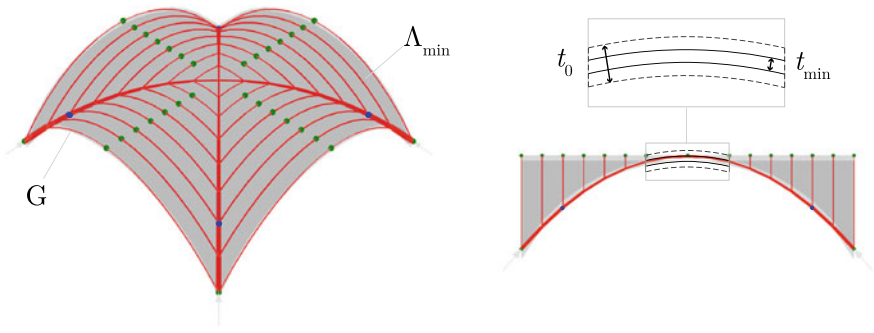


Fig. 4.7 Minimum thickness solution for the shallow vault with thickness  $t_{min} = 0.151$  m resulting in a GSF of 3.3

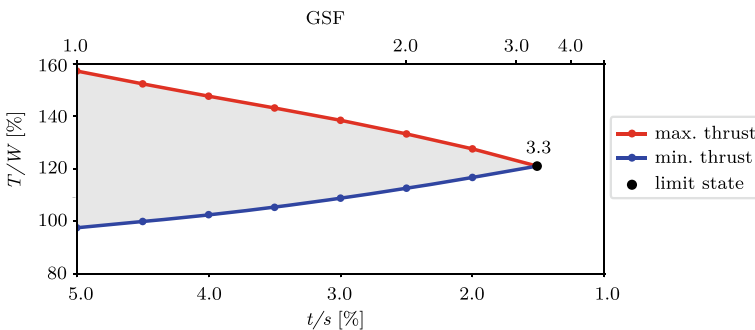
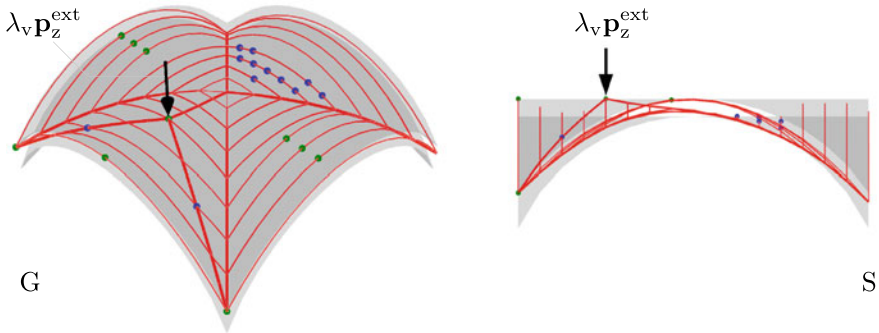


Fig. 4.8 Stability domain obtained for the shallow cross vault plotting the normalised thrust-overweights ( $T/W$ ) for decreasing normalised structural thicknesses ( $t/s$ )



**Fig. 4.9** Results for optimising a concentrated vertical load applied to the middle of the web for an orthogonal form diagram added with a direct force path to the supports. The maximum vertical load multiplier is  $\lambda_v^{\max} = 121.8$  resulting in a load-over-total-weight of  $P_{\max}/W=11.2\%$

discussed in Maia Avelino et al. (2021b), Nodargi and Bisegna (2022), different form diagrams can be compared to enlarge this stability domain and obtain a larger GSF.

#### 4.4.4 Maximum Vertical Load Multiplier

The maximisation of a concentrated vertical load is studied in this Section. The cross vault is subjected to an off-centred unitary pointed load  $\mathbf{p}_z^{\text{ext}} [n \times 1]$  applied in the middle of the structural web  $(x_p, y_p) = (5.0, 2.5)$ . The auxiliary variable  $\lambda_v \geq 0$  representing the vertical load multiplier is considered to model this problem. For the present problem,  $\mathbf{p}_z^{\text{ext}}$  has zero entries to all but the position related to the vertex  $(x_p, y_p)$ , which has entry  $-1.0$  representing an additional load pointing downwards.

To account for the additional load, the form diagram used in Sects. 4.4.2–4.4.3 is modified by adding a direct path from the point of load application  $(x_p, y_p)$  to the adjacent supports.

The optimisation is performed to minimise Eq. 4.12. It results in a maximum applied load multiplier  $\lambda_v^{\max} = 121.8$ , i.e., a maximum applied load  $P_{\max} = 121.8$  kN, resulting in a load-over-total-weight of  $P_{\max}/W = 11.2\%$ . The thrust network obtained and the force diagram are depicted in Fig. 4.9. The concentrated load flows to the supports through the added lines. Looking at the sectional view, the point where the load is applied is discontinuous, and the network touches the extrados (green dot).

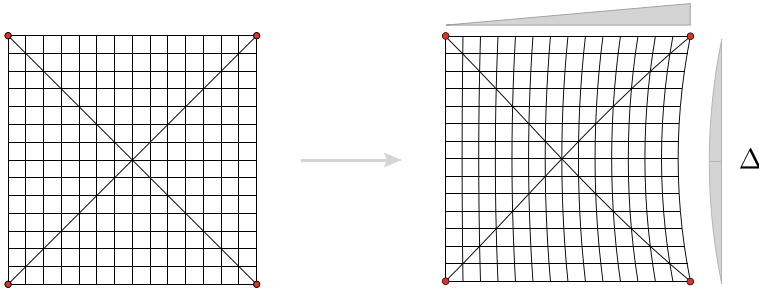


**Fig. 4.10** Diagram modification by applying a tapered curved profile to the nodes of the form diagram to enable the application of horizontal loads with  $\Delta = 5\%$  of the span

### 4.4.5 Maximum Horizontal Load Multiplier

This section presents the problem of computing the maximum horizontal load multiplier at the shallow cross vault. The vector defining the loading case  $\mathbf{p}_h^{\text{ext}}$  assigns a force in the  $x$ -direction at every node with the same magnitude as the lumped self-weight ( $p_{z,i}$ ) applied to that node. An additional variable  $\lambda_h \geq 0$  is considered to represent the horizontal load multiplier, i.e. a fraction of the vertical load applied horizontally.

The form diagram used for the analysis is modified with a curved profile and maximum magnitude equal to  $\Delta = 5\%$  of the span. This sliding transformation can be seen as the equivalent of tilting the planar diagram to respond to the horizontal loads. This transformation is depicted in Fig. 4.10.

The optimisation problem is solved again using the objective function in Eq. 4.13. The maximum value obtained for this problem is  $\lambda_h^{\text{max}} = 0.179$ , meaning that the maximum horizontal-load-over-weight applied to the cross vault is equal to  $P_{\text{max}}/W = 17.9\%$ . The solution is depicted in Fig. 4.11.

This problem is relevant to modelling, e.g., the static equivalent of seismic forces in masonry vaults (Dejong, 2009). It also corresponds to tilting the vault by a giving rotation angle such that a fraction of the weight is applied horizontally (Zessin, 2012). The maximum horizontal load multiplier obtained depends on the form diagram chosen and the sliding magnitude  $\Delta$  applied. Hence, further modifications and new topologies should be coupled to this problem, considering alternative internal force distributions.

### 4.4.6 Internal State Under Support Displacements

This section discusses the problem of subjecting the vault to a support settlement. By minimising the complementary energy (Eq. 4.14) of the structure subjected to a given support displacement  $\bar{\mathbf{u}}$ , a stress state can be found compatible with  $\bar{\mathbf{u}}$  (Angelillo,

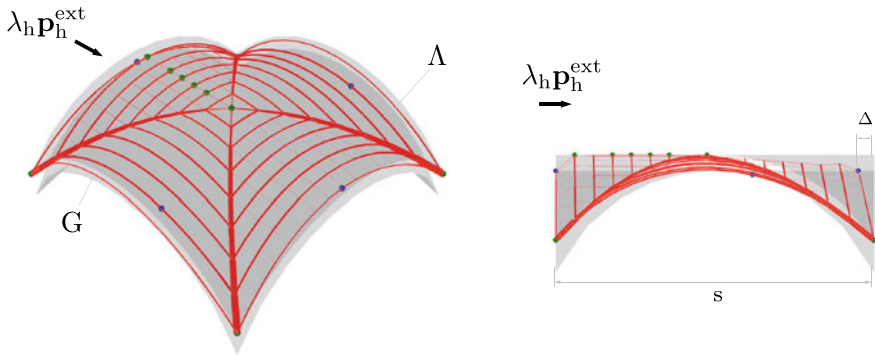


**Fig. 4.11** Results for maximising the horizontal load multiplier  $\lambda_h^{\max} = 0.179$ , resulting in a normalised horizontal force  $P_{\max}/W = 17.9\%$  applied to the cross vault with a horizontal slide of the nodes of the pattern equal to  $\Delta/s = 5\%$

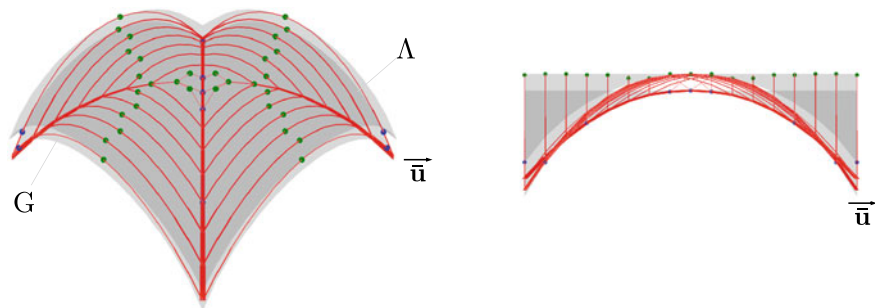


**Fig. 4.12** Thrust network (G) obtained for the optimisation minimising the complementary energy subjected to a unit diagonal settlement in the highlighted support  $\bar{\mathbf{u}}$ . The objective function value is  $W_c = 266.9$  kNm

2014; Iannuzzo et al., 2018, 2020). The shallow cross vault is subjected to a unitary outward diagonal displacement applied to one of the vault's support  $\bar{\mathbf{u}}$  (see Fig. 4.12). The thrust network obtained and extreme points touching intrados and extrados are depicted in Fig. 4.12.

The optimal complementary energy value is  $W_c = 266.9$  kNm i.e.,  $W_c/W = 20.4\%$ . The outward diagonal displacement reflects a spreading of the webs crossing the pulled diagonal. This spreading reflects into two crack lines crossing that diagonal, obtained by connecting adjacent vertices touching the extrados (green). Qualitatively, the crack lines in the webs described follow the crack pattern obtained in cross vaults with Discrete Element Modelling (DEM) in McInerney and DeJong (2015).

Minimising the complementary energy shows how cracks are induced at the onset of support displacements. Future work can rely on TNO analysis to study the inverse problem of determining the foundation displacements that resulted in the cracked configuration observed in general vaulted masonry structures. The crack location

can then be used to inform reinforcing strategies if necessary (De Santis et al., 2019; Fugger et al., 2022).

### 4.4.7 Towards the Application of TNA in Surveyed Buildings

This final section highlights the potential of applying the TNA framework directly to the scanned geometries of surveyed buildings. The case of St. Angelo Church in Anagni, Italy (Maia Avelino et al., 2022b) is revisited and summarised in Fig. 4.13. Given TNA’s simple input requirement, the analysis can be performed based on the geometry acquired, and the pipeline for the analysis is described herein.

The geometry is acquired through photogrammetry or laser scanning surveys, and the vault’s intrados and extrados surfaces are extracted to generate the optimisation constraints (see Eqs. 4.8). Finding a suitable form diagram for an existing, distorted, highly constrained structural envelope is challenging. Currently, the patterning of such diagrams follows the designer’s experience following the structure’s geometric features, curvature, openings and cracks. In Fig. 4.13b, five different diagram

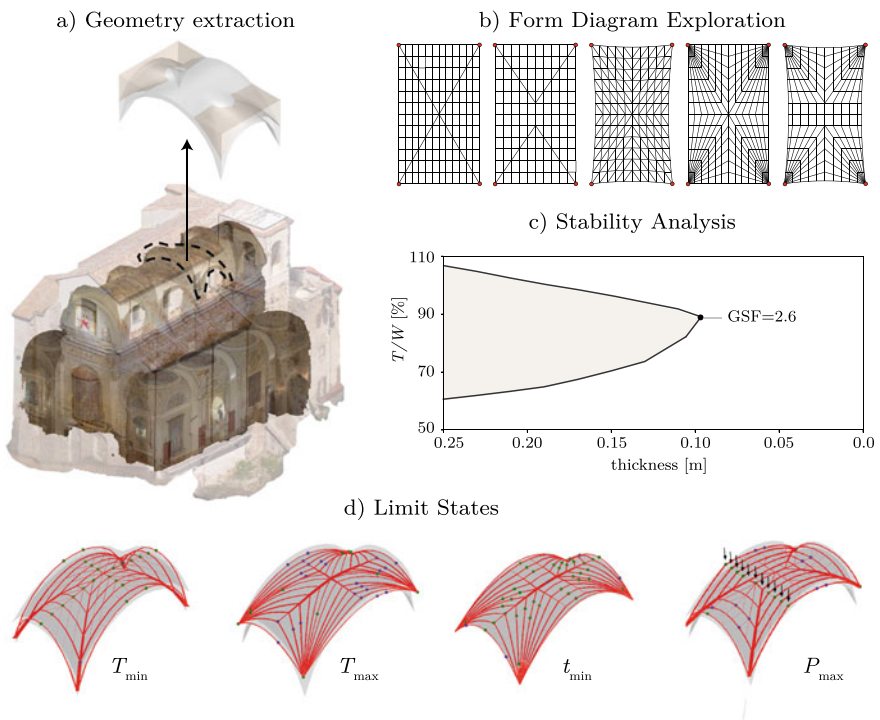


**Fig. 4.13** Pipeline for the TNA stability analysis from geometry obtained from scanned data. Case study at the St. Angelo Church, in Anagni, Italy

topologies are used to investigate the structure's stability domain. The domain is computed considering the envelope of these diagrams as shown in Fig. 4.13c. The stability domain obtained is a lower bound of the structure's actual space of allowable stresses. Further form diagrams can be added to the analysis to expand such domains. A series of limit states can also be computed, e.g., the minimum ( $T_{\min}$ ) and maximum ( $T_{\max}$ ) thrust states, the minimum thickness ( $t_{\min}$ ) and collapse load cases ( $P_{\max}$ ).

The modular multi-objective framework presented in this book chapter enables these analyses that could be readily applied to isolated vaults of scanned heritage buildings. Future research will focus on improving or automating the definition of form diagrams to the analyses and considering the global structural stability of the building, taking into account its laterally supporting structure and the interaction between adjacent vaulted elements in the structure.

## 4.5 Conclusions

This chapter reviews Thrust Network Analysis (TNA) approaches for masonry structures based on limit analysis. TNA enables finding admissible stress states in masonry structures by formulating suitable constrained optimisation problems. Admissible stress states in masonry structures correspond to compressive networks within the structure's geometry.

A novel modular multi-objective optimisation framework is presented in this chapter, which enables finding multiple particular solutions in masonry structures with a single approach. Among these solutions are the minimum and maximum horizontal thrusts, the minimum structural thickness (or maximum Geometric Safety Factor), the maximum vertical and horizontal collapse loads, and the effect of foundation settlements. These particular solutions are obtained by considering different objective functions. By combining these states, a complete picture of the level of stability of the structure can be obtained. Furthermore, it can give information about crack patterns after applying additional loads or support movements.

Finally, recent activity on lower-bound equilibrium methods, including continuous and discrete methods, such as TNA, and the development of novel open-source computational tools based on these methods has the potential to impact the field by increasing the number of assessment tools available to analyse heritage masonry structures.

Nevertheless, multiple challenges and open questions remain, such as how to overcome the specificity of the form diagram and provide engineers with adapted or automatically generated diagrams for the analysis or how to extend the analysis to the building scale, obtaining global structural safety factors. Future work should also ease working with scanned data obtained from existing buildings to leverage TNA's simple geometry-based input and enhance its applications in practical assessment scenarios.

## References

- Aita, D., Pedemonte, O., & Williams, K. (eds.) (2015). *Masonry structures: Between mechanics and architecture* (1st ed.). Springer International Publishing. ISBN 978-3-319-13003-3. <https://doi.org/10.1007/978-3-319-13003-3>.
- Aita, D., Barsotti, R., & Bennati, S. (2019). A parametric study of masonry domes equilibrium via a revisit of the Durand-clay method. In *Proceedings of the 7th International Conference on Computational Methods in Structural Dynamics and Earthquake Engineering (COMP-DYN 2015), Crete, Greece, 2019* (pp. 663–672). Institute of Structural Analysis and Antiseismic Research School of Civil Engineering National Technical University of Athens (NTUA) Greece. ISBN 978-618-82844-5-6. <https://doi.org/10.7712/120119.6947.19313>.
- Angelillo, M. (2014). Practical applications of unilateral models to Masonry Equilibrium. In F. Pfeiffer, F. G. Rammerstorfer, E. Guazzelli, B. Schrefler, P. Serafini, & M. Angelillo (Eds.), *Mechanics of masonry structures* (Vol. 551, pp. 109–210). Springer. ISBN 978-3-7091-1773-6 978-3-7091-1774-3. [https://doi.org/10.1007/978-3-7091-1774-3\\_4](https://doi.org/10.1007/978-3-7091-1774-3_4).
- Angelillo, M., Babilio, E., & Fortunato, A. (2013). Singular stress fields for masonry-like vaults. *Continuum Mechanics and Thermodynamics*, 25(2–4), 423–441. ISSN 09351175. <https://doi.org/10.1007/s00161-012-0270-9>.
- Angelillo, M., Fortunato, A., Gesualdo, A., Iannuzzo, A., & Zuccaro, G. (2018). Rigid block models for masonry structures. *International Journal of Masonry Research and Innovation*, 3(4), 349, 2018. ISSN, 2056–9459, 2056–9467. <https://doi.org/10.1504/IJMRI.2018.095701>
- Angelillo, M., Olivieri, C., & DeJong, M. J. (2021). A new equilibrium solution for masonry spiral stairs. *Engineering Structures*, 238, 112176. ISSN 01410296. <https://doi.org/10.1016/j.engstruct.2021.112176>.
- Baker, S. J., Horne, M. R., & Heyman, J. (January 1956). *The steel skeleton* (Vol. 2). Plastic Behaviour and Design: Cambridge University Press. 978-0-521-04088-4
- Bhooshan, S., Bhooshan, V., Dell'Endice, A., Chu, J., Singer, P., Megens, J., Van Mele, T., & Block, P. (2022). The Striatore bridge. *Architecture, structures and construction*. ISSN 2730-9894. <https://doi.org/10.1007/s44150-022-00051-y>.
- Block, P. (2009). *Thrust network analysis: Exploring three-dimensional equilibrium*. Ph.D. thesis, Massachusetts Institute of Technology. <https://dspace.mit.edu/handle/1721.1/49539>.
- Block, P., & Lachauer, L. (2014). Three-dimensional funicular analysis of masonry vaults. *Mechanics Research Communications*, 56, 53–60. ISSN 00936413. <https://doi.org/10.1016/j.mechrescom.2013.11.010>.
- Block, P., & Ochsendorf, J. (2007). Thrust network analysis: A new methodology for 3D equilibrium. *Journal of the International Association for Shell and Spatial Structures*, 48(155), 1–7. ISSN 1028-365X.
- Block, P., & Ochsendorf, J. (2002). Lower-bound analysis of masonry vaults (1892).
- Block, P., Van Mele, T., Liew, A., DeJong, M., & Escobedo, D. (2018). Structural design, fabrication and construction of the Armadillo vault - the institution of structural engineers. *The Structural Engineer*, 96(5), 10–20. [https://www.istructe.org/journal/volumes/volume-96-\(2018\)/issue-5/structural-design-fabrication-and-construction-of/](https://www.istructe.org/journal/volumes/volume-96-(2018)/issue-5/structural-design-fabrication-and-construction-of/).
- Block, P., Calvo Barentin, C., Ranaudo, F., & Paulson, N. (2019). Imposing challenges, disruptive changes: Rethinking the floor slab
- Block Research Group. RhinoVault 2 (2021). <https://github.com/BlockResearchGroup/compas-RV2>
- Bruggi, M. (2020). A constrained force density method for the funicular analysis and design of arches, domes and vaults. *International Journal of Solids and Structures*, 193–194, 251–269. ISSN 00207683. <https://doi.org/10.1016/j.ijsolstr.2020.02.030>.
- Chiozzi, A., Milani, G., & Tralli, A. (2017). A genetic algorithm NURBS-based new approach for fast kinematic limit analysis of masonry vaults. *Computers and Structures*, 182, 187–204. ISSN 00457949. <https://doi.org/10.1016/j.compstruc.2016.11.003>.
- Culmann, K. (1875). *Die graphische statik*. Meyer and Zeller (A. Reimann), Zurich.

- Cundall, P. (1971). A computer model for simulating progressive, large-scale movements in blocky rock systems. *International Journal of Rock Mechanics, Mining Sciences, and Geomechanics Abstracts*, 25(3), 107–116. <https://www.semanticscholar.org/paper/A-computer-model-for-simulating-progressive%2C-in-Cundall/b185b3a85160c3a77ec30e6b6e8d2e2e6de82033>.
- D’Altri, A. M., Sarhosis, V., Milani, G., Rots, J., Cattari, S., Lagomarsino, S., Sacco, E., Tralli, A., Castellazzi, G., & de Miranda, S. (2019). Modeling strategies for the computational analysis of unreinforced masonry structures: Review and classification. *Archives of Computational Methods in Engineering*. ISSN 18861784. <https://doi.org/10.1007/s11831-019-09351-x>.
- De Santis, S., de Felice, G., & Roscini, F. (2019). Retrofitting of masonry vaults by basalt textile-reinforced mortar overlays. *International Journal of Architectural Heritage*, 13(7), 1061–1077. ISSN 1558-3058. <https://doi.org/10.1080/15583058.2019.1597947>.
- Dejong, M. J. (2009). *Seismic assessment strategies for masonry structures*. Ph.D. thesis, MIT, Cambridge.
- Fantin, M., & Ciblac, T. (2016). Extension of thrust network analysis with joints consideration and new equilibrium states. *International Journal of Space Structures*, 31(2–4), 190–202. ISSN 20598033. <https://doi.org/10.1177/0266351116661814>.
- Fraddosio, A., Lepore, N., & Piccioni, M. D. (2019). *Lower bound limit analysis of masonry vaults under general load conditions*. Springer International Publishing. ISBN 978-3-319-99440-6. <https://doi.org/10.0>.
- Fraddosio, A., Lepore, N., & Piccioni, M. D. (2020). Thrust surface method: An innovative approach for the three-dimensional lower bound Limit Analysis of masonry vaults. *Engineering Structures*, 202(October 2019), 109846. ISSN 18737323. <https://doi.org/10.1016/j.engstruct.2019.109846>.
- Fraternali, F. (2010). A thrust network approach to the equilibrium problem of unreinforced masonry vaults via polyhedral stress functions. *Mechanics Research Communications*, 37(2), 198–204. ISSN 00936413. <https://doi.org/10.1016/j.mechrescom.2009.12.010>.
- Fugger, R., Maia Avelino, R., Iannuzzo, A., Block, P., & de Felice, G. (2022). A new numerical limit analysis-based strategy to retrofit masonry curved structures with FRCM systems. In *The 8th European Congress on Computational Methods in Applied Sciences and Engineering*, 5–9 June 2022, Oslo, Norway.
- Funari, M. F., Silva, L. C., Mousavian, E., & Lourenço, P. B. (2021). Real-time structural stability of domes through limit analysis: Application to St. Peter’s dome. *International Journal of Architectural Heritage*, 1–23. ISSN 1558-3058. <https://doi.org/10.1080/15583058.2021.1992539>.
- Grillanda, N., Chiozzi, A., Milani, G., & Tralli, A. (2019). Collapse behavior of masonry domes under seismic loads: An adaptive NURBS kinematic limit analysis approach. *Engineering Structures*, 200, 109517. ISSN 18737323. <https://doi.org/10.1016/j.engstruct.2019.109517>.
- Heyman, J. (1966). The stone skeleton. *International Journal of Solids and Structures*, 2(2), 249–279. ISSN 00207683. [https://doi.org/10.1016/0020-7683\(66\)90018-7](https://doi.org/10.1016/0020-7683(66)90018-7).
- Heyman, J. (1969). The safety of masonry arches. *International Journal of Mechanical Sciences*, 11(4), 363–385. ISSN 00207403. [https://doi.org/10.1016/0020-7403\(69\)90070-8](https://doi.org/10.1016/0020-7403(69)90070-8).
- Heyman, J. (1995). *The stone skeleton*. Cambridge University Press. ISBN 978-0-521-47270-8. <https://doi.org/10.1017/CBO9781107050310>.
- Huerta, S. (2008). The analysis of masonry architecture: A historical approach. *Architectural Science Review*, 51(4), 297–328. <https://doi.org/10.3763/asre.2008.5136>
- Iannuzzo, A., Angelillo, M., De Chiara, E., De Guglielmo, F., De Serio, F., Ribera, F., & Gesualdo, A. (2018). Modelling the cracks produced by settlements in masonry structures. *Meccanica*, 53(7), 1857–1873. ISSN 0025-6455, 1572-9648. <https://doi.org/10.1007/s11012-017-0721-2>.
- Iannuzzo, A., Van Mele, T., Block, P. (2020). Piecewise rigid displacement (PRD) method: A limit analysis-based approach to detect mechanisms and internal forces through two dual energy criteria. *Mechanics Research Communications*, 107, 103557. ISSN 00936413. <https://doi.org/10.1016/j.mechrescom.2020.103557>.
- Lemos, J. V. (2007). Discrete element modeling of masonry structures. *International Journal of Architectural Heritage*, 1(2), 190–192. ISSN 1558-3058. <https://doi.org/10.1080/15583050601176868>.

- Lemos, J. V. (2019). Discrete element modeling of the seismic behavior of masonry construction. *Buildings*, 9(2), 43. ISSN 2075-5309. <https://doi.org/10.3390/buildings9020043>.
- Liew, A., Pagonakis, D., Van Mele, T., & Block, P. (2018). Load-path optimisation of funicular networks. *Meccanica*, 53(1–2), 279–294. ISSN 0025-6455. <https://doi.org/10.1007/s11012-017-0714-1>.
- Liew, A., Avelino, R., Moosavi, V., Van Mele, T., Block, P. (2019). Optimising the load path of compression-only thrust networks through independent sets. *Structural and Multidisciplinary Optimization*, 60(1), 231–244. ISSN 1615-147X. <https://doi.org/10.1007/s00158-019-02214-w>.
- LimitState Ltd. Limit State:RING - Industry Leading Masonry Arch Analysis Software | Limit State (2020). <https://www.limitstate.com/ring>.
- Lourenço, P. B., & Rots, J. G. (1997). Multisurface interface model for analysis of masonry structures. *Journal of Engineering Mechanics*, 123(7), 660–668. ISSN 0733-9399. [https://doi.org/10.1061/\(ASCE\)0733-9399\(1997\)123:7\(660\)](https://doi.org/10.1061/(ASCE)0733-9399(1997)123:7(660)).
- Maia Avelino, R. (2023). Compas TNO: Finding admissible thrust networks in vaulted masonry structures. <https://doi.org/10.5281/zenodo.7895617>.
- Maia Avelino, R. (2023). Thrust network optimisation for the assessment of vaulted masonry structures. Ph.D. thesis, ETH Zurich, Zurich, 2023. <https://doi.org/10.3929/ethz-b-000611351>.
- Maia Avelino, R., Iannuzzo, A., Van Mele, T., & Block, P. (2021a). Assessing the safety of vaulted masonry structures using thrust network analysis. *Computers & Structures*, 257, 106647. ISSN 00457949. <https://doi.org/10.1016/j.compstruc.2021.106647>.
- Maia Avelino, R., Iannuzzo, A., Van Mele, T., & Block, P. (2021b). Parametric stability analysis of groin vaults. *Applied Sciences*, 11(8), 3560. ISSN 2076-3417. <https://doi.org/10.3390/app11083560>.
- Maia Avelino, R., Iannuzzo, A., Van Mele, T., & Block, P. (2022a). An energy-based strategy to find admissible thrust networks compatible with foundation settlements in masonry structures. *Mechanics Research Communications*, 125, 103978. ISSN 0093-6413. <https://doi.org/10.1016/j.mechrescom.2022.103978>.
- Maia Avelino, R., Olivieri, C., Donval, E., Fugger, R., Lai, M., Saretta, Y., Weichbrodt, A., & Sangirardi, M. (2022b). An integrated approach to the structural assessment of historic buildings: The case of St. Angelo Church in Anagni. *Structural*, 241. <https://doi.org/10.12917/STRU241.13>.
- McInerney, J., & DeJong, M. J. (2015). Discrete element modeling of groin vault displacement capacity. *International Journal of Architectural Heritage*, 9(8), 1037–1049. ISSN 1558-3058. <https://doi.org/10.1080/15583058.2014.923953>.
- Mehrotra, A., Liew, A., Block, P., & DeJong, M. J. (2023). An integrated modelling approach for the seismic collapse assessment of masonry towers. *International Journal of Architectural Heritage*, 17(1), 90–113. ISSN 1558-3058. <https://doi.org/10.1080/15583058.2022.2139207>.
- Milani, E., Milani, G., & Tralli, A. (2008). Limit analysis of masonry vaults by means of curved shell finite elements and homogenization. *International Journal of Solids and Structures*, 45(20), 5258–5288. ISSN 00207683. <https://doi.org/10.1016/j.ijsolstr.2008.05.019>.
- Moseley, H. (1843). On the theory of the arch. Practice and architecture of bridges. In J. Weale (Ed.), *Theory* (pp. 1–72). Architectural Library.
- Nodargi, N. A. & Bisegna, P. (2022). Generalized thrust network analysis for the safety assessment of vaulted masonry structures. *Engineering Structures*, 270, 114878. ISSN 0141-0296. <https://doi.org/10.1016/j.engstruct.2022.114878>.
- Obvis. (2016). ArchieM. Version 2.5.1. Obvis Ltd. <http://www.obvis.com/archie-m/>.
- O'Dwyer, D. (1999). Funicular analysis of masonry vaults. *Computers & Structures*, 73(1–5), 187–197. ISSN 00457949. [https://doi.org/10.1016/S0045-7949\(98\)00279-X](https://doi.org/10.1016/S0045-7949(98)00279-X).
- Parisi, F., Balestrieri, C., & Varum, H. (2019). Nonlinear finite element model for traditional adobe masonry. *Construction and Building Materials*, 223, 450–462. ISSN 0950-0618. <https://doi.org/10.1016/j.conbuildmat.2019.07.001>.

- Poleni, G. Memorie storiche della gran cupola del tempio vaticano, e de'danni di essa, e de'ristoramenti loro, divise in libri cinque ... Stamperia del Seminario, Padova, 1748. <https://doi.org/10.3931/e-rara-13403>.
- Prager, W. (1959). *An introduction to plasticity*. Addison-Wesley Publishing Company.
- Rippmann, M. (2016). Funicular shell design: Geometric approaches to form finding and fabrication of discrete funicular structures. Ph.D. thesis, ETH Zurich, Zurich.
- Rippmann, M., Lachauer, L., & Block, P. (2012). Interactive vault design. *International Journal of Space Structures*, 27(4), 219–230. ISSN 0266-3511. <https://doi.org/10.1260/0266-3511.27.4.219>.
- Schek, H. J. (1974). The force density method for form finding and computation of general networks. *Computer Methods in Applied Mechanics and Engineering*, 3(1), 115–134. ISSN 00457825. [https://doi.org/10.1016/0045-7825\(74\)90045-0](https://doi.org/10.1016/0045-7825(74)90045-0).
- Shin, H. V., Porst, C. F., Vouga, E., Ochsendorf, J., & Durand, F. (2016). Reconciling elastic and equilibrium methods for static analysis. *ACM Transactions on Graphics*, 35(2), 1–16. ISSN 0730-0301. <https://doi.org/10.1145/2835173>.
- Smars, P. (2000). Sur La Stabilité Des Arcs et Voutes. Ph.D. thesis, KULeuven.
- Smoljanović, H., Živaljić, N., & Nikolić, Ž. (2013). A combined finite-discrete element analysis of dry stone masonry structures. *Engineering Structures*, 52, 89–100. ISSN 0141-0296. <https://doi.org/10.1016/j.engstruct.2013.02.010>.
- Tralli, A., Alessandri, C., & Milani, G. (2014). Computational methods for masonry vaults: A review of recent results. *The Open Civil Engineering Journal*, 8(1), 272–287. ISSN 1874-1495. <https://doi.org/10.2174/1874149501408010272>.
- Ungewitter, G. (1890). *Lehrbuch Der Gotischen Konstruktionen*. Leipzig: T.O. Weigel Nachfolger.
- Van Mele, T., & Block, P. (2014). Algebraic graph statics. *CAD Computer Aided Design*, 53, 104–116. ISSN 00104485. <https://doi.org/10.1016/j.cad.2014.04.004>.
- Wächter, A., & Biegler, L. T. (2006). On the implementation of an interior-point filter line-search algorithm for large-scale nonlinear programming. *Mathematical Programming*, 106(1), 25–57. ISSN 0025-5610. <https://doi.org/10.1007/s10107-004-0559-y>.
- Wolfe, W. S. (1921). *Graphical analysis: A text book in graphic statics*. New York: McGraw-Hill Book Company.
- Zessin, J., Lau, W., & Ochsendorf, J. (2010). Equilibrium of cracked masonry domes. *Proceedings of the Institution of Civil Engineers: Engineering and Computational Mechanics*, 163(3), 135–145. ISSN 17550777. <https://doi.org/10.1680/eacm.2010.163.3.135>.
- Zessin, J. F. (2012). Collapse analysis of unreinforced masonry domes and curving walls. Ph.D. thesis, MIT, Cambridge. <http://dspace.mit.edu/handle/1721.1/70879>.